



Supplement of

Dimethyl sulfide chemistry over the industrial era: comparison of key oxidation mechanisms and long-term observations

Ursula A. Jongebloed et al.

Correspondence to: Ursula A. Jongebloed (ujongebl@uw.edu) and Becky Alexander (beckya@uw.edu)

The copyright of individual parts of the supplement might differ from the article licence.

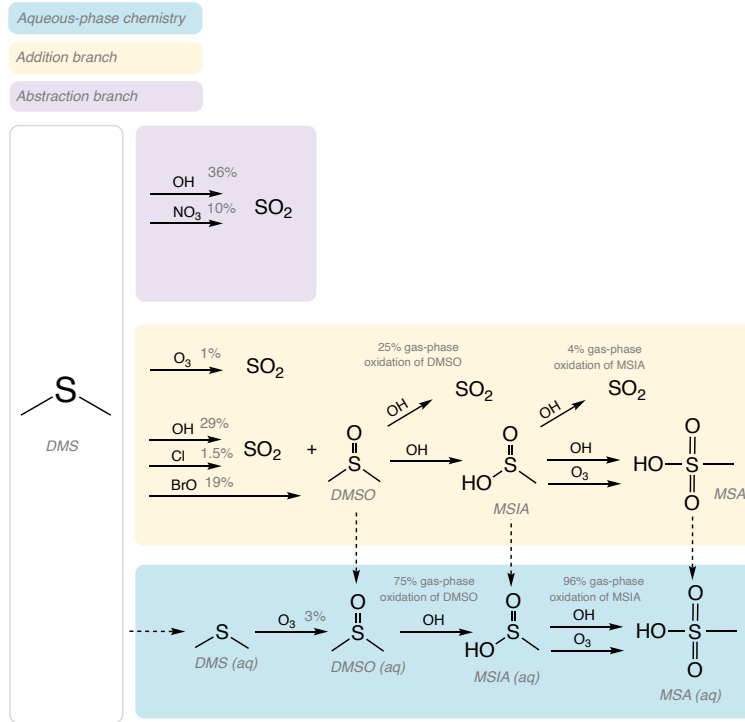


Figure S1. The DMS oxidation chemistry in the Q. Chen mechanism implemented by Chen et al. (2018), which includes aqueous-phase chemistry, important intermediates such as dimethyl sulfoxide (DMSO, CH_3SOCH_3) and methanesulfinic acid (MSIA, $\text{CH}_3\text{SO}_2\text{H}$), and reaction of DMS with halogen oxidants Cl and BrO. Reaction rates and a detailed description of the mechanism can be found in Chen et al. (2018).

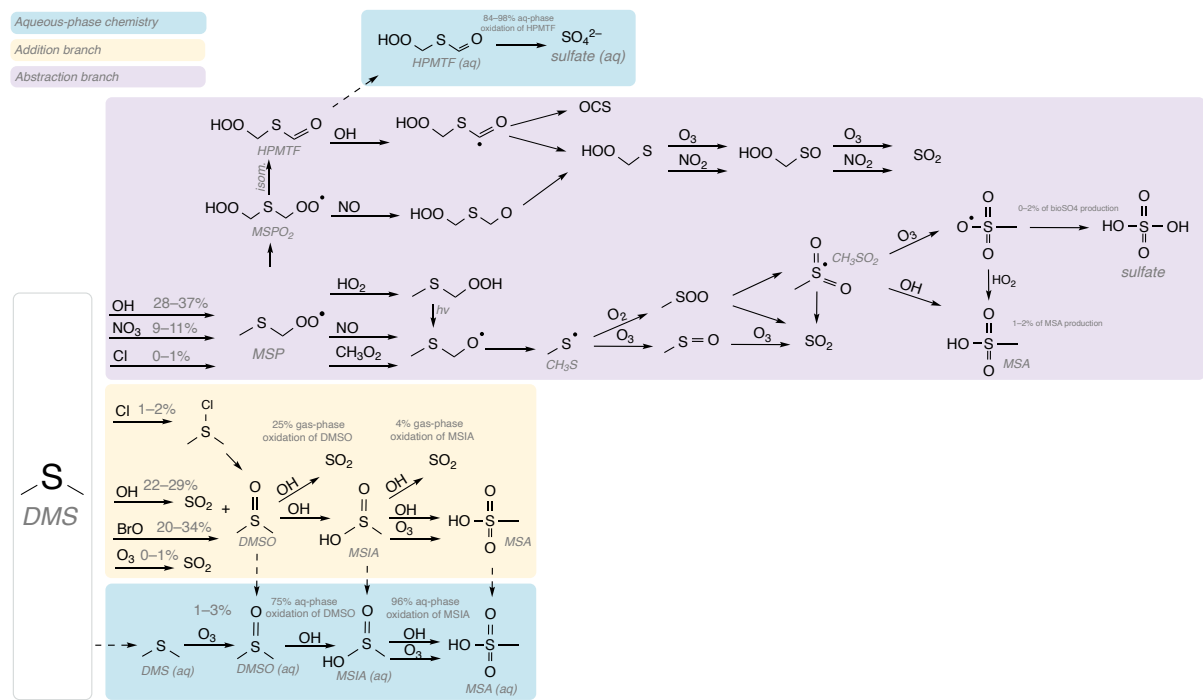


Figure S2. DMS oxidation chemistry in the Tashmim mechanism, originally implemented by Tashmim et al. (2024). This mechanism includes aqueous-phase chemistry, intermediates, and halogen reactions from Chen et al. (2018) as well as updates to the abstraction pathway, such as the formation of HPMTF and aqueous-phase formation of sulfate from HPMTF. Reaction rates and other mechanism details can be found in Tashmim et al. (2024).

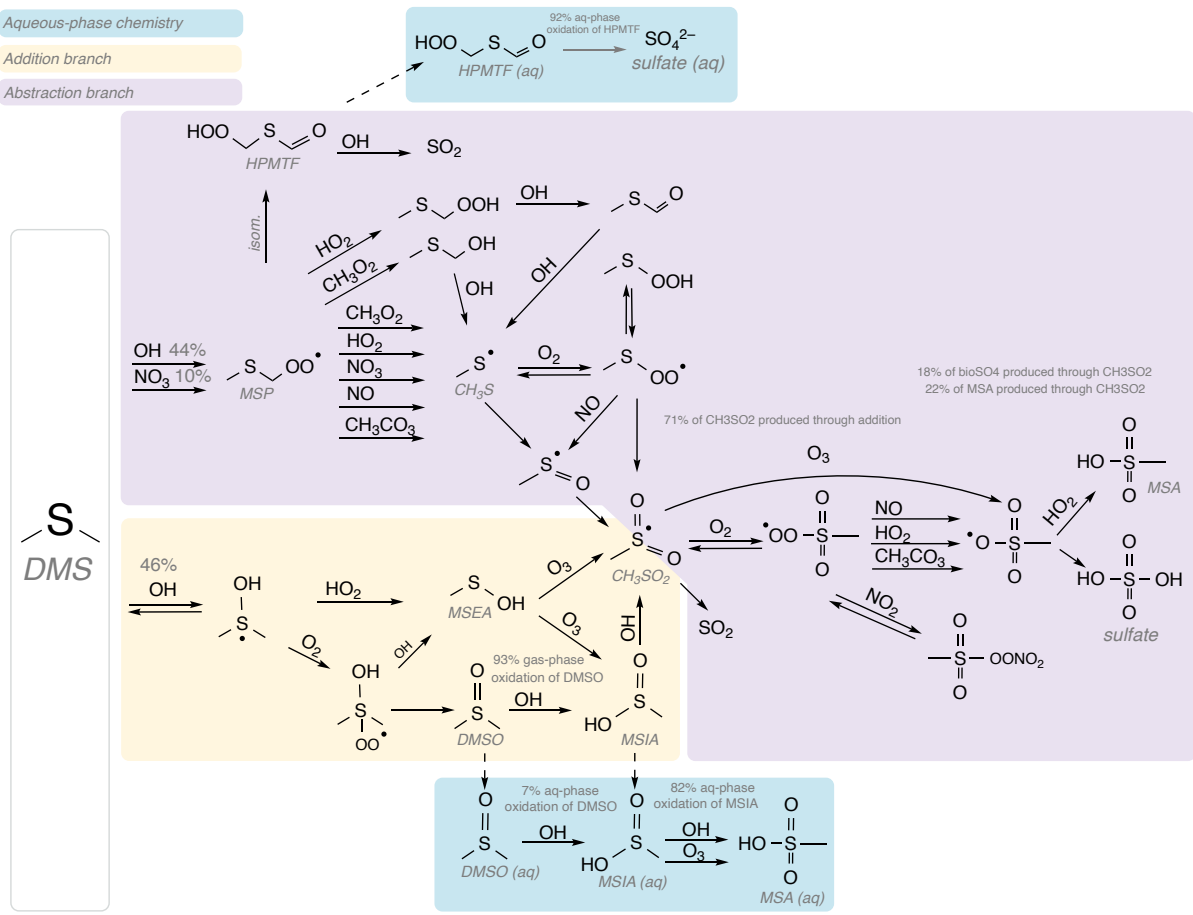


Figure S3. DMS oxidation chemistry in GEOS-Chem for the J. Chen mechanism, which includes aqueous-phase chemistry from Chen et al. (2018) and Tashmim et al. (2024) and gas-phase chemistry from Chen et al. (2023). Henry's law constants for all aqueous-phase species are from Chen et al. (2023) (see Table S1). Reaction rates and other mechanism details can be found in Chen et al. (2023).

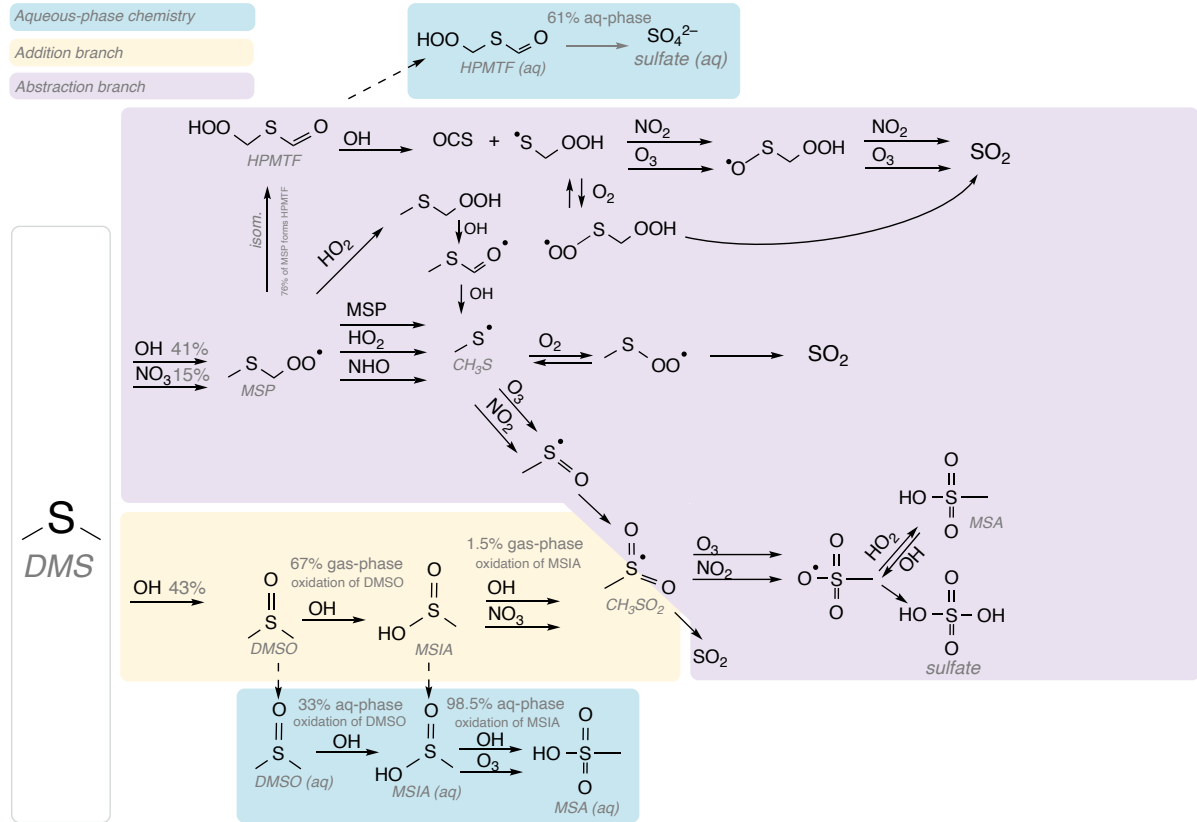


Figure S4. DMS oxidation chemistry in GEOS-Chem for the Cala mechanism, which includes aqueous-phase chemistry from Chen et al. (2018) and Tashmim et al. (2024) and gas-phase chemistry from Cala et al. (2023). Henry's law constants for all aqueous-phase species are from Tashmim et al. (2024) (see Table S1). Reaction rates and other mechanism details can be found in Cala et al. (2023).

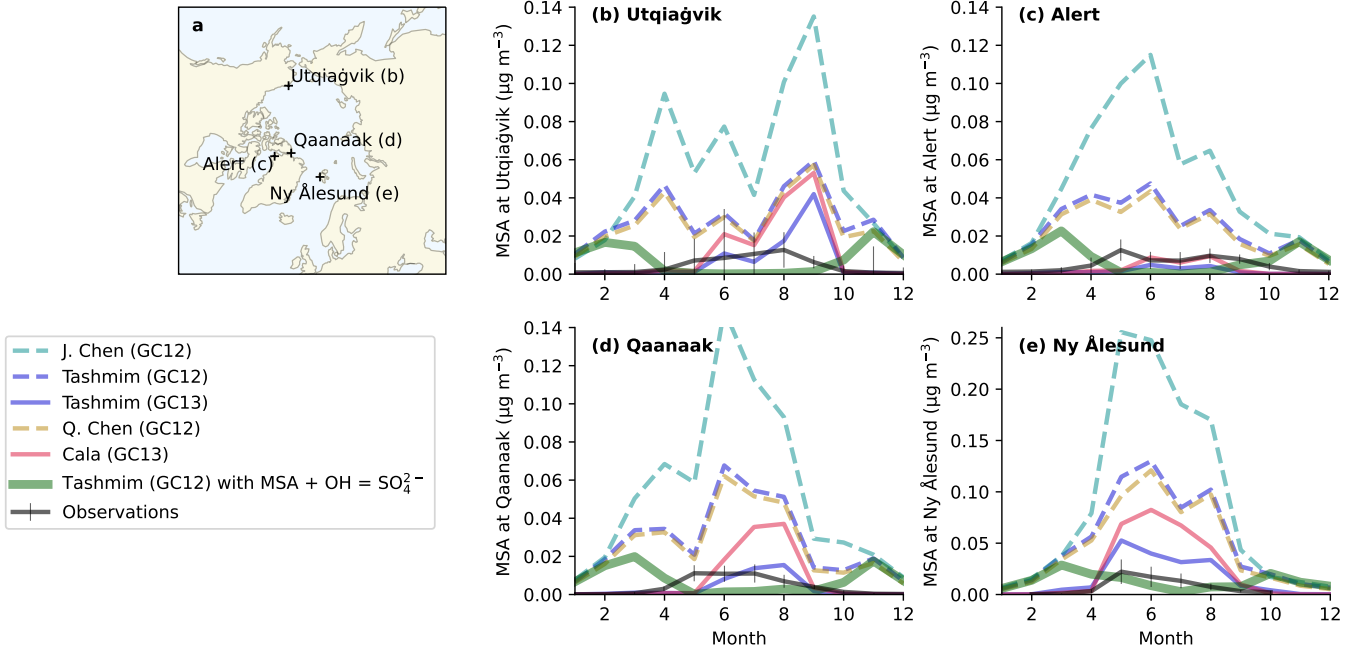


Figure S5. Same as Fig. 8, but we also show the Tashmim (GC12) simulation with $\text{MSA} + \text{OH} (\text{aq}) \rightarrow \text{SO}_4^{2-}$ from Chen et al. (2018) (dark green line). Including the aqueous-phase destruction of MSA by OH causes MSA concentrations to peak in the fall and spring and reach a minimum in the summer, which is the opposite of the observed seasonality (black lines). This reaction is likely a minor loss process in aerosol and is not expected to occur in cloud droplets (Mungall et al., 2018), but in both Fung et al. (2022) and Tashmim et al. (2024) mechanism, about 75% of MSA is converted to sulfate in the aqueous phase.

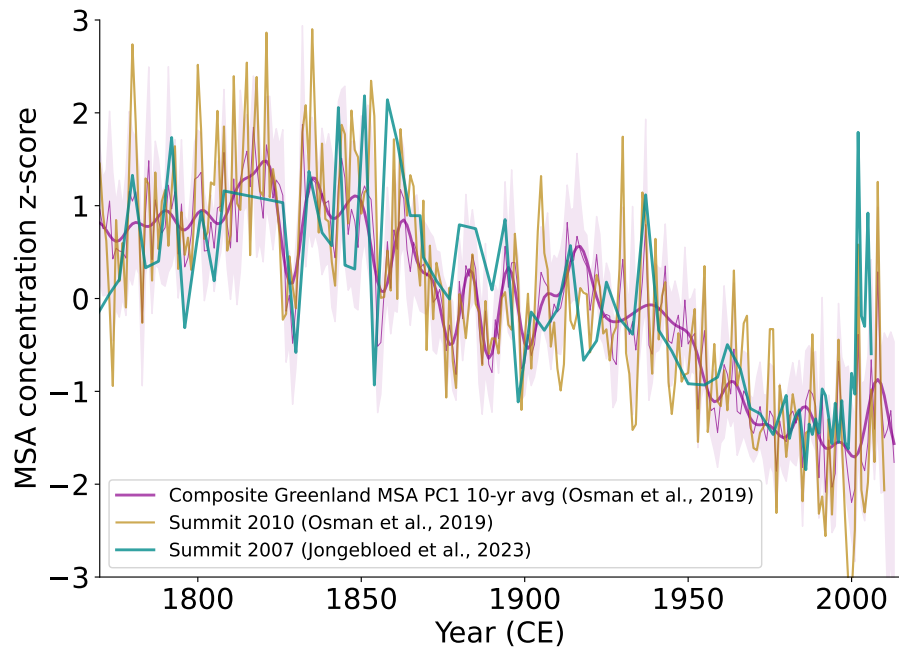


Figure S6. Z-score of MSA concentrations in 12 ice cores from across the Greenland ice sheet (pink line) and the 95th percentile confidence interval (pink shading) (Osman et al., 2019). Additionally, Z-score of MSA concentrations in two Summit ice cores in green (Jongebloed et al., 2023a) and gold (Osman et al., 2019).

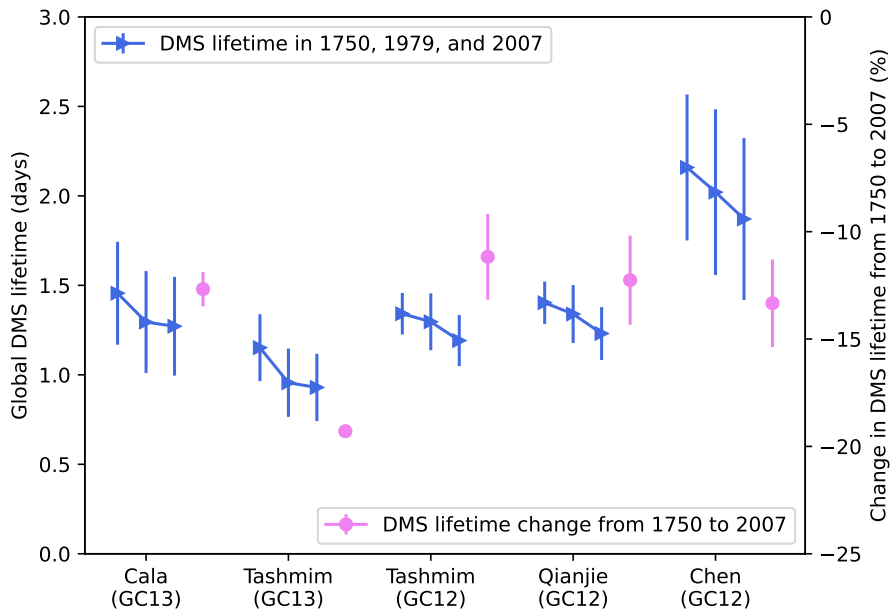


Figure S7. Global mean DMS atmospheric lifetime in each simulation in Table S1, where the left blue triangle is the 1750 simulation, the middle blue triangle is the 1979 simulation, and the right blue triangle is the 2007 simulation. The pink dot shows the percent change in global mean DMS lifetime between the 1750 and 2007 simulation for each mechanism.

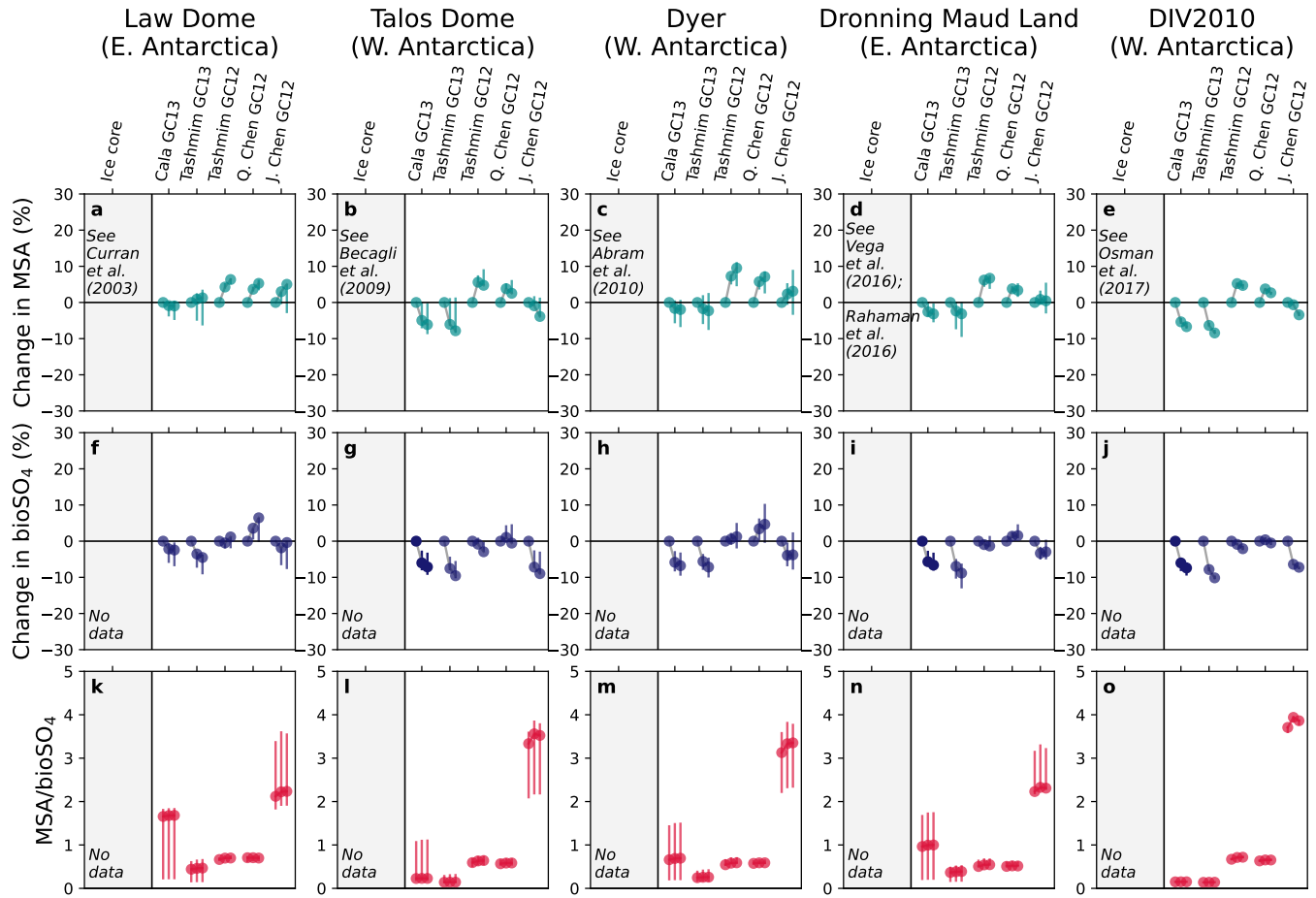


Figure S8. Same as Figure 4, but for the locations of five Antarctic ice cores from previously published studies, including Law Dome (Curran et al., 2003), Talos Dome (Becagli et al., 2009), Dyer (Abram et al., 2010), Dronning Maud Land (Rahaman et al., 2016; Vega et al., 2016), and DIV2010 (Osman et al., 2017). Left markers in a-j indicate the 1750 simulation percent change relative to 1750 (always zero). Middle markers in a-j represent the percent difference in MSA and bioSO₄ between the 1979 and 1750 simulations. Right markers in a-j represent the percent difference between the 2007 and 1750 simulations. In k-o, the left markers are 1750 MSA/bioSO₄, middle markers are 1979 MSA/bioSO₄, and right markers are 2007 MSA/bioSO₄. We do not compute the changes in MSA deposition from ice core observations because observations are not available online in most references (e.g., Curran et al., 2003; Becagli et al., 2009; Rahaman et al., 2016; Osman et al., 2017).

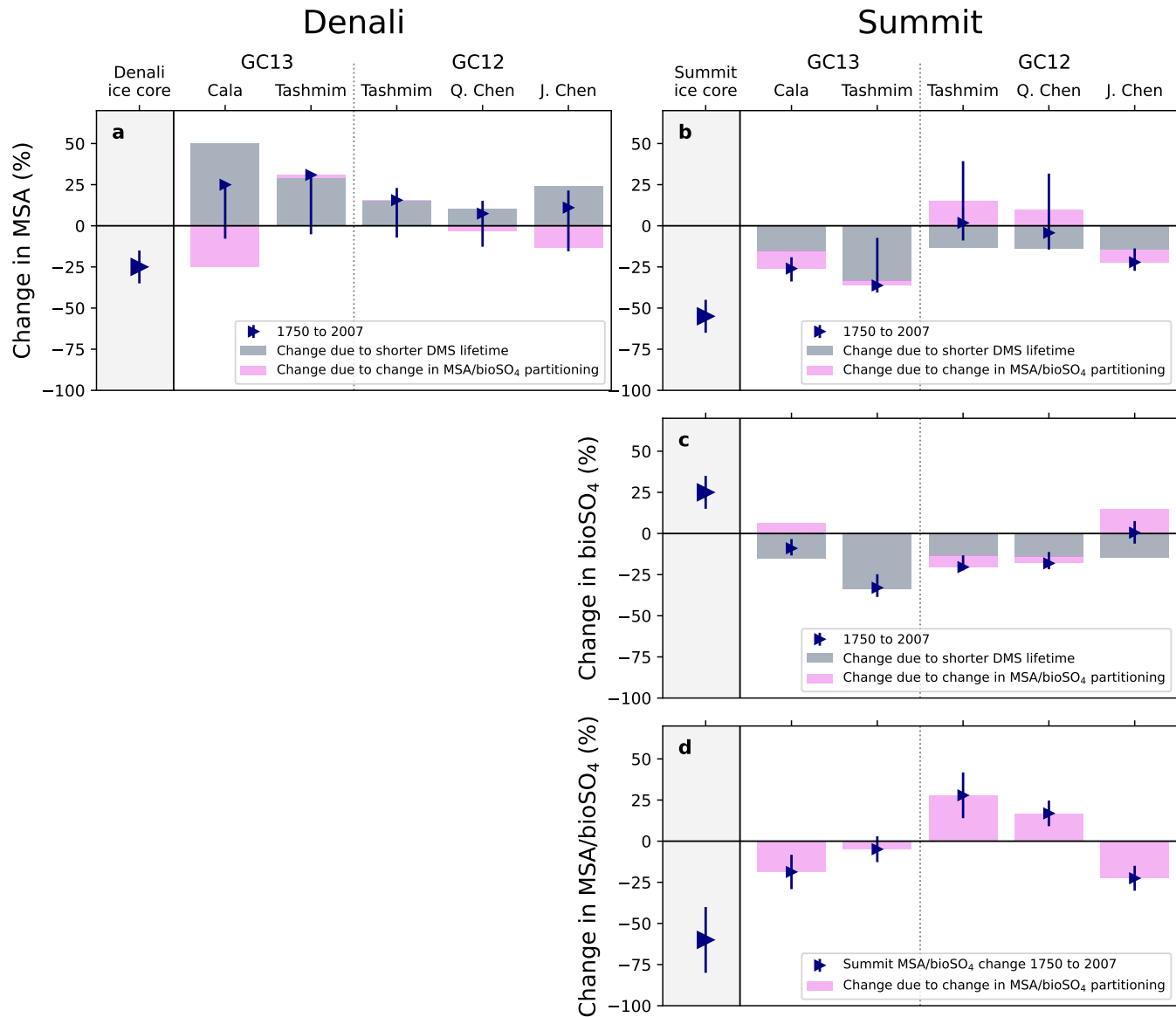


Figure S9. The same as Fig. 7, but showing changes between 1750 and 2007 instead of 1750 to 1979.

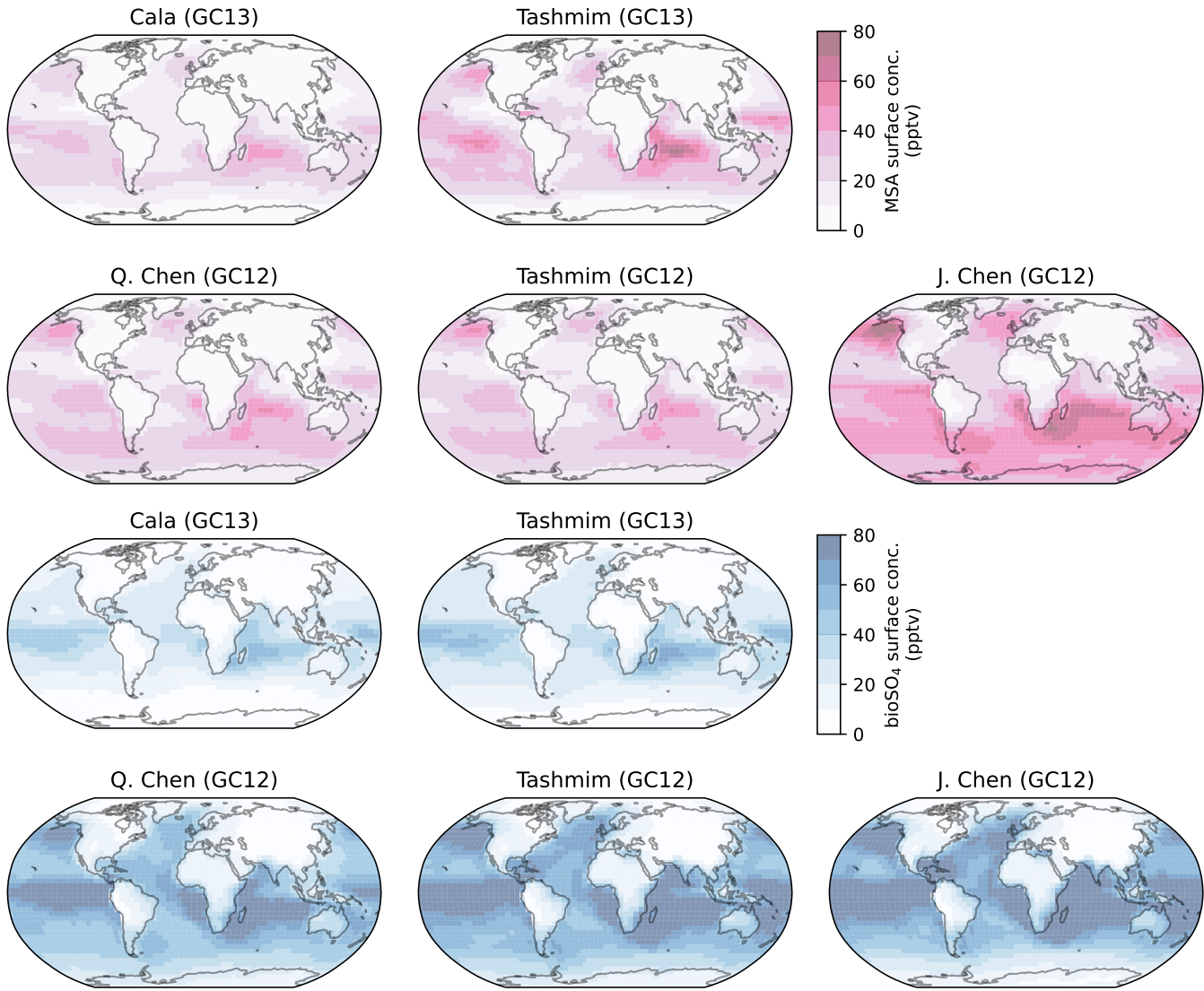


Figure S10. Annual mean surface MSA (top) and bioSO_4 (bottom) concentrations in each simulation described in Table 1.

Table S1. Henry's law constants of aqueous-phase intermediates in J. Chen vs. Tashmim, Q. Chen, and Cala mechanisms.

Compound	J. Chen mechanism		Tashmim, Q. Chen, and Cala mechanisms	
	$-\Delta H/R$ [K]	$H_X(298)$ [$M\text{ atm}^{-1}$]	$-\Delta H/R$ [K]	$H_X(298)$ [$M\text{ atm}^{-1}$]
DMS	3100	0.48	4480	0.56
DMSO	3100	1×10^4	2580	1×10^7
MSIA	3100	1×10^8	1760	1×10^8
MSEA	3100	1×10^7	N/A	N/A
HPMTF	3100	1×10^4	5200	1×10^3

Table S2. Global MSA budget calculations. Atmospheric lifetime is estimated by dividing atmospheric burden by loss (wet + dry deposition).

Year	Mechanism	Production	Dry Deposition	Wet Deposition	Burden	Lifetime
		($Tg\text{ S yr}^{-1}$)	($Tg\text{ S yr}^{-1}$)	($Tg\text{ S yr}^{-1}$)	($Tg\text{ S}$)	(days)
1750	Q. Chen (GC12)	3.47	0.60	2.88	0.29	2.55
1979	Q. Chen (GC12)	3.62	0.63	2.99	0.29	2.50
2007	Q. Chen (GC12)	3.53	0.62	2.92	0.28	2.47
1750	Tashmim (GC13)	4.70	0.61	4.10	0.21	1.40
1979	Tashmim (GC13)	4.65	0.61	4.10	0.21	1.40
2007	Tashmim (GC13)	4.70	0.61	4.10	0.21	1.40
1750	Tashmim (GC12)	3.46	0.59	2.86	0.30	2.74
1979	Tashmim (GC12)	3.50	0.63	3.01	0.31	2.66
2007	Tashmim (GC12)	3.58	0.62	2.95	0.30	2.61
1750	J. Chen (GC12)	6.70	0.96	5.75	0.73	3.37
1979	J. Chen (GC12)	6.62	0.96	5.67	0.87	4.09
2007	J. Chen (GC12)	6.49	0.96	5.54	0.82	3.93
1750	Cala (GC13)	4.49	0.46	4.07	0.21	1.43
1979	Cala (GC13)	4.30	0.45	3.91	0.20	1.42
2007	Cala (GC13)	4.28	0.45	3.89	0.20	1.41

Table S3. Global DMS-derived sulfate (bioSO_4) budget calculations.

Year	Mechanism	Production (Tg S yr $^{-1}$)	Dry Deposition (Tg S yr $^{-1}$)	Wet Deposition (Tg S yr $^{-1}$)	Burden (Tg S)	Lifetime (days)
1750	Q. Chen (GC12)	8.57	1.88	7.33	0.85	2.87
1979	Q. Chen (GC12)	8.46	1.75	7.28	0.83	2.84
2007	Q. Chen (GC12)	8.53	1.78	7.41	0.81	2.74
1750	Tashmim (GC13)	7.95	1.03	6.51	0.35	1.44
1979	Tashmim (GC13)	7.95	1.03	6.51	0.35	1.44
2007	Tashmim (GC13)	7.95	1.03	6.51	0.35	1.44
1750	Tashmim (GC12)	9.69	1.73	8.15	0.85	2.65
1979	Tashmim (GC12)	9.55	1.66	8.03	0.82	2.63
2007	Tashmim (GC12)	9.65	1.70	8.15	0.81	2.56
1750	J. Chen (GC12)	9.28	1.43	7.65	0.55	1.89
1979	J. Chen (GC12)	9.38	1.46	7.70	0.68	2.29
2007	J. Chen (GC12)	9.53	1.52	7.87	0.69	2.26
1750	Cala (GC13)	6.11	0.79	5.22	0.31	1.59
1979	Cala (GC13)	6.40	0.76	5.42	0.31	1.56
2007	Cala (GC13)	6.42	0.76	5.44	0.31	1.55

5 References

- Abram, N. J., Thomas, E. R., McConnell, J. R., Mulvaney, R., Bracegirdle, T. J., Sime, L. C., and Aristarain, A. J.: Ice core evidence for a 20th century decline of sea ice in the Bellingshausen Sea, Antarctica, *Journal of Geophysical Research: Atmospheres*, 115, <https://doi.org/10.1029/2010JD014644>, 2010.
- Becagli, S., Castellano, E., Cerri, O., Curran, M., Frezzotti, M., Marino, F., Morganti, A., Proposito, M., Severi, M., Traversi, R., and Udisti, R.: Methanesulphonic acid (MSA) stratigraphy from a Talos Dome ice core as a tool in depicting sea ice changes and southern atmospheric circulation over the previous 140 years, *Atmospheric Environment*, 43, 1051–1058, <https://doi.org/10.1016/j.atmosenv.2008.11.015>, 2009.
- Cala, B. A., Archer-Nicholls, S., Weber, J., Abraham, N. L., Griffiths, P. T., Jacob, L., Shin, Y. M., Revell, L. E., Woodhouse, M., and Archibald, A. T.: Development, intercomparison, and evaluation of an improved mechanism for the oxidation of dimethyl sulfide in the UKCA model, *Atmospheric Chemistry and Physics*, 23, 14 735–14 760, <https://doi.org/10.5194/acp-23-14735-2023>, 2023.
- Chen, J., Lane, J. R., Bates, K. H., and Kjaergaard, H. G.: Atmospheric Gas-Phase Formation of Methanesulfonic Acid, *Environmental Science and Technology*, <https://doi.org/10.1021/acs.est.3c07120>, 2023.
- Chen, Q., Sherwen, T., Evans, M., and Alexander, B.: DMS oxidation and sulfur aerosol formation in the marine troposphere: A focus on reactive halogen and multiphase chemistry, *Atmospheric Chemistry and Physics*, 18, 13 617–13 637, <https://doi.org/10.5194/acp-18-13617-2018>, 2018.
- Curran, M. A. J., van Ommen, T. D., Morgan, V. I., Phillips, K. L., and Palmer, A. S.: Ice Core Evidence for Antarctic Sea Ice Decline Since the 1950s, *Science*, 302, 1203–1206, <https://doi.org/https://doi.org/10.1126/science.1087888>, 2003.
- Fung, K. M., Heald, C. L., Kroll, J. H., Wang, S., Jo, D. S., Gettelman, A., Lu, Z., Liu, X., Zaveri, R. A., Apel, E. C., Blake, D. R., Jimenez, J. L., Campuzano-Jost, P., Veres, P. R., Bates, T. S., Shilling, J. E., and Zawadowicz, M.: Exploring dimethyl sulfide (DMS) oxidation and implications for global aerosol radiative forcing, *Atmospheric Chemistry and Physics*, 22, 1549–1573, <https://doi.org/10.5194/acp-22-1549-2022>, 2022.
- Jongebloed, U. A., Schauer, A. J., Cole-Dai, J., Lerrick, C. G., Porter, W. C., Tashmim, L., Zhai, S., Salimi, S., Edouard, S. R., Geng, L., and Alexander, B.: Industrial-era decline in Arctic methanesulfonic acid is offset by increased biogenic sulfate aerosol, *Proceedings of the National Academy of Sciences*, 120, <https://doi.org/10.1073/pnas.2307587120>, 2023a.
- Mungall, E. L., Wong, J. P., and Abbatt, J. P.: Heterogeneous Oxidation of Particulate Methanesulfonic Acid by the Hydroxyl Radical: Kinetics and Atmospheric Implications, *ACS Earth and Space Chemistry*, 2, 48–55, <https://doi.org/10.1021/acsearthspacechem.7b00114>, 2018.
- Osman, M., Das, S. B., Marchal, O., and Evans, M. J.: Methanesulfonic acid (MSA) migration in polar ice: Data synthesis and theory, *Cryosphere*, 11, 2439–2462, <https://doi.org/10.5194/tc-11-2439-2017>, 2017.
- Osman, M. B., Das, S. B., Trusel, L. D., Evans, M. J., Fischer, H., Grieman, M. M., Kipfstuhl, S., McConnell, J. R., and Saltzman, E. S.: Industrial-era decline in subarctic Atlantic productivity, *Nature*, 569, 551–555, <https://doi.org/10.1038/s41586-019-1181-8>, 2019.
- Rahaman, W., Thamban, M., and Laluraj, C.: Twentieth-century sea ice variability in the Weddell Sea and its effect on moisture transport: Evidence from a coastal East Antarctic ice core record, *The Holocene*, 26, 338–349, <https://doi.org/10.1177/0959683615609749>, 2016.
- Tashmim, L., Porter, W. C., Chen, Q., Alexander, B., Fite, C. H., Holmes, C. D., Pierce, J. R., Croft, B., and Ishino, S.: Contribution of expanded marine sulfur chemistry to the seasonal variability of dimethyl sulfide oxidation products and size-resolved sulfate aerosol, *Atmospheric Chemistry and Physics*, 24, 3379–3403, <https://doi.org/10.5194/acp-24-3379-2024>, 2024.

Vega, C. P., Schlosser, E., Divine, D. V., Kohler, J., Martma, T., Eichler, A., Schwikowski, M., and Isaksson, E.: Surface mass balance and water stable isotopes derived from firn cores on three ice rises, Fimbul Ice Shelf, Antarctica, *The Cryosphere*, 10, 2763–2777, <https://doi.org/10.5194/tc-10-2763-2016>, 2016.